Advances and Applications in Mathematical Sciences
Volume 19, Issue 12, October 2020, Pages 1279-1307

UNSTEADY FLOW OF JEFFREY NANOFLUID: A NUMERICAL SIMULATION BY BIVARIATE SIMPLE ITERATION METHOD

O. OTEGBEYE[1], Md. S. ANSARI[2], T. P. SINGH[2], M. TRIVEDI[2] and S. P. GOQO[1]

[1]School of Mathematics
Statistics and Computer Science
University of KwaZulu-Natal
Pietermaritzburg, South Africa
E-mail: muyiwabowen@yahoo.com
goqo@ukzn.ac.za

[2]School of Technology
Pandit Deendayal Petroleum University
Gandhinagar-382007, India
E-mail: shariffuddin@gmail.com
tajinder.singh@spt.pdpu.ac.in
mumukshu.tphd15@sot.pdpu.ac.in

Abstract

A new numerical algorithm termed as bivariate simple iteration method (BSIM) for nonlinear and coupled systems/PDEs is exercised on unsteady magneto hydrodynamic flow of Jeffrey nanofluid past stretching surface taking into account; temperature dependent thermal conductivity, non-linear radiation and viscous dissipation. This numerical algorithm involves implementation of relaxation on nonlinear system of equations, which is accomplished by taking all linear functions to be unknown functions for granted while defining nonlinear functions as both known (previously defined initial solution that satisfies the boundary conditions) and unknown. Mass transfer is analysed by imposing impact of first order chemical reaction. Equations, modeling the flow, are non-dimensionalised by implementing compatible transformations and retained in homogeneous form. Convergence of proposed method are substantiated by analysing solution and residual errors. It is found to converge rapidly and yields accurate results. Analysis reveals that strength of chemical reaction perturbs the diffusion rate, resulting a decrease in nanoparticle concentration.

2010 Mathematics Subject Classification: 76A05, 76W05, 65N35, 76V05.

Keywords: Bi-variate simple iteration method, Jeffrey nanouid, Magnetic field, Nonlinear radiation effect, Chemical reaction.

Received November 2, 2020; Accepted January 2020

1. Introduction

In vast domain of fluid mechanics, Non-Newtonian fluid has taken preeminent position in upbringing of recent technology and substantial industrial applications [1, 2, 3, 4, 5, 6, 7]. Different model of non-Newtonian fluids are available in literature, because of its diversified constitutive relationship that alone cannot characterize all types of non-Newtonian fluids. Entire domain of non-Newtonian fluids is mainly classified into these three subsets viz. (i) differential type, (ii) rate type and (iii) integral type. Fluid currently under consideration lies in rate type fluid, termed as Jeffrey fluid which incorporates relaxation and retardation time. Idea of retardation of fluid flow was first of all appealed by Jeffery while analysing wave propagation in earth's mantle using Jeffery temperature flux model. The time taken by the fluid to restore to its primary stable state is relaxation time. Moreover, finding an analytic solution of the governing Navier-Stoke's equations, coupled with energy and concentration equations, describing the flow dynamics of non-Newtonian type nanofluid are extremely challenging.

Nanofluid having a great potential in heat and mass transfer, due to its physical structure, apprehends it's applications in the field of: coal slurries, drawing rubber sheets and mixture of clays, coolant in nuclear reactors, *X*-rays, computers etc. [8, 9, 10]. Having higher heat absorption rate than its base fluid, nanofluid lie under the category of super coolants. Nanofluid dramatically boosts thermal conductivity of base liquids, without any shortcoming as pressure drop, coagulation, erosion and sedimentation [11, 12, 35]. This in turn, boosts their performance, ultimately benefits in building miniaturized devices having high cooling ability. Theearliest observations of thermal conductivity enhancement of nanofluid were projected in 1993 by Masuda et al. [13]. The term "nanofluid" was pioneered by Choi [14], about a few decades ago, to indicate engineered colloidal fluids composed by doping the base fluid with nanoparticles. Theoretically, the finer the particles, the bigger the surface area for transferring the heat which subsequently enhances the heat-efficiency of suspended particles as a function of heat exchange surfaces. A viscoelastic nanofluid partaking an

lead on Maxwell's model because of its characteristics of relaxation to retardation time is Jeffrey Nanofluid. In recent years, investigations of Jeffrey nanofluid is found to be elevated, because of its more realistic behaviour while taking part in various types of practical applications. Shahzad et al. [15] conducted a study on flow of Jeffrey fluid with nanoparticles at stretching sheet with viscous, Joule and magnetic field effects. Abbasi et al. [16] addressed mixed convective flow of magneto hydrodynamic Jeffrey nanofluid considering effect of radiation, double stratifications. Hayat et al. [17] explored magneto hydrodynamic flow of Jeffrey nanofluid sloseby nonlinear stretching surface subjected to convective condition and heat generation/absorption. Hayat et al. [18] reported a convergent solution of Jeffrey nanofluid flow with actively and passively controlled nano-particle concentration at stretching boundary. Shehzad et al [19] explored a study on MHD flow of Jeffrey nanofluid at a boundary stretching bidirectionally. Magneto hydrodynamic flow of Jeffrey nanofluid induced due to exponential stretcthing of boundary was looked by Hussain et al. [20]. Abbasi et al. [4] investigated hydromagnetic flow of Jeffrey nanofluid on stretching sheet employing conditions on heat and mass flux. Bhatti et al. [21] considered effects of coagulation on MHD peristaltically generated motion of Jeffrey nanofluid plus gyrotactic microorganism. Entropy analysis in convective Poiseulle type flow of Molybdenum Disulphide Jeffrey Nanofluid was viewed by Gul et al. [22]. Hasona [23] investigated temperature dependent viscosity on peristaltic flow of Jeffrey nanofluid on asymmetric channel. Khan et al. [24] disclosed a report on heat transfer phenomena of Jeffrey nanofluid at inclined stretching sheet using generalised laws of Fourier and Fick. Saleem et al. [25] explored a mixed convection of Jeffrey nanofluid adjacent to rotating cone with magnetic field and gyrotactic microorganisms. Pal et al. [26] presented an analysis dealing entropy generation and radiation of convective magneto hydrodynamic Jeffrey nanofluid flow at stretching boundary. Ali et al. [27] studied unsteady magneto hydrodynamic rotational flow of Jeffrey nanofluid near a plate in porous medium. Recently, Ansari et al. [28] reported the effects of temperature dependent thermal conductivity on MHD Jeffrey nanofluid stretched flow near a Riga plate.

Following the studies [29, 30, 31, 32, 33, 34, 35, 36], we intend to examine the unsteady magneto hydrodynamic Jeffrey nanofluid flow at an impulsively stretching surface adding viscous heating and variable thermal conductivity. Nonlinear radiation is considered as this is defensible for high as well as low temperature variations whereas linear radiation is workable only for low temperature variation. First order chemical reactions (assuming destructive) are included. Chemical reaction phenomenon appears in electrochemistry, chemical industries, hydrolysis, combustion processes and electro-plating. To best of author's knowledge, such model for flow and heat characteristics comprising the above effects doesn't appear in literature. The focus of the investigation is also to test the applicability of the proposed method (BSIM) on non-linear and coupled PDEs arising in flow problems. Description of method in context with considered flow problem is presented. Physical interpretation and convergence of numerical scheme are discussed. The method is found to be efficient in giving accurate results. Novelty of the present work is to introduce bi-variate simple iteration method on the model characterising magneto hydrodynamic Jeffrey nanofluid flow over an impulsively stretching surface along with simultaneous effects of viscous dissipation, variable thermal conductivity and non linear radiation.

2. Mathematical Formulation

Flow analysis is carried on variable thermal conductivity, nonlinear radiation, chemical reaction and viscous dissipation on unsteady boundary layer flow of Jeffrey nanofluid at impulsively stretching sheet in vertically upward direction (i.e. x axis). The temperature and nanoparticle concentration at surface is considered to be higher than that of free stream. A magnetic field B is imposed in normal direction of stretching sheet (i.e. y axis). The flow conservation together with boundary layer approximations give equations characterising the present problem [20]:

$$\frac{\partial \Lambda_1}{\partial x} + \frac{\partial \Lambda_2}{\partial y} = 0, \tag{1}$$

$$\frac{\partial \Lambda_1}{\partial x} = \frac{v\lambda_2}{\gamma}\left(\frac{\partial^3 \Lambda_1}{\partial y^2 \partial t} + \Lambda_1 \frac{\partial^3 \Lambda_1}{\partial x \partial y^2} + \Lambda_2 \frac{\partial^3 \Lambda_1}{\partial y^3} - \frac{\partial \Lambda_1}{\partial x}\frac{\partial^2 \Lambda_1}{\partial y^2} + \frac{\partial \Lambda_1}{\partial y} + \frac{\partial \Lambda_1}{\partial y}\frac{\partial^2 \Lambda_1}{\partial x \partial y}\right)$$

$$-\left(\Lambda_1 \frac{\partial \Lambda_1}{\partial x} + \Lambda_2 \frac{\partial \Lambda_1}{\partial y}\right) + \frac{\nu}{\gamma}\frac{\partial^2 \Lambda_1}{\partial y^2} - \frac{\sigma}{\rho c_p} B^2 \Lambda_1 \tag{2}$$

$$\frac{\partial H}{\partial t} + \Lambda_1 \frac{\partial H}{\partial x} + \Lambda_2 \frac{\partial H}{\partial y} = \frac{1}{\rho c_p}\frac{\partial}{\partial y}\left(k \frac{\partial H}{\partial y}\right) + \tau_p\left[D_B \frac{\partial E}{\partial y}\frac{\partial H}{\partial y} + \frac{D_H}{H_\infty}\left(\frac{\partial H}{\partial y}\right)^2\right]$$

$$-\frac{1}{\rho c_p}\frac{\partial q_r}{\partial y} + \frac{\nu}{c_p \gamma}\left(\frac{\partial \Lambda_1}{\partial y}\right)^2 + \frac{v\lambda_2}{c_p \gamma}\left(\Lambda_1 \frac{\partial \Lambda_1}{\partial y}\frac{\partial^2 \Lambda_1}{\partial x \partial y} + \frac{\partial \Lambda_1}{\partial y}\frac{\partial^2 \Lambda_1}{\partial t \partial y} + \Lambda_2 \frac{\partial \Lambda_1}{\partial y}\frac{\partial^2 \Lambda_1}{\partial^2 y}\right), \tag{3}$$

$$\frac{\partial E}{\partial t} + \Lambda_1 \frac{\partial E}{\partial x}\Lambda_2 \frac{\partial E}{\partial y} = D_B \frac{\partial^2 E}{\partial y^2} + \frac{D_H}{H_\infty}\frac{\partial^2 H}{\partial y^2} - k_c(E - E_\infty), \tag{4}$$

where, $\tau_p = (\rho c)_p/(\rho c)_f$, $\gamma = 1 + \lambda_1 \cdot \Lambda_1(x, y)$ and $\Lambda_2(x, y)$ are velocity in $x-$ and $y-$ directions. $H(x, y)$: temperature, $E(x, y)$: nanoparticle concentration. λ_1, λ_2, k_c, D_B, and D_H, are, respectively, ratio of relaxation to retardation time, relaxation time, chemical reaction rate, Brownian and thermophoresis diffusion.

Associated conditions are

$$t < 0 : \forall x,\ y\, \Lambda_1 = 0, \Lambda_2 = 0,\ H = H_\infty,\ E = E_\infty, \tag{5}$$

$$t \geq 0 : \begin{cases} At\ y = 0 : \Lambda_1 = \Lambda_{1w}(x) = \alpha x;\ \Lambda_2 = 0;\ H = H_w;\ E = E_w, \\ At\ y \to \infty : \Lambda_1 \to 0; \frac{\partial \Lambda_1}{\partial y} \to 0;\ H = H_\infty;\ E \to E_\infty \end{cases} \tag{6}$$

a is constant. Nonlinear radiation flux :

$$q_r = \frac{4\sigma^*}{3k^*}\frac{\partial H^4}{\partial y} = \frac{16\sigma^*}{3k^*} H^3 \frac{\partial H}{\partial y}, \tag{7}$$

where, σ^* : Stefan-Boltzmann constant, k^* : Rosseland absorption coefficient. Using (7) in (3), the energy equation (3) takes following form:

$$\frac{\partial H}{\partial} - \frac{v}{c_p\gamma}\left(\frac{\partial \Lambda_1}{\partial y}\right)^2 \frac{1}{\rho c_p}\frac{\partial}{\partial y}\left(k + \frac{16\sigma^*}{3k^*}H^3\frac{\partial H}{\partial y}\right) + \tau\left[D_B\frac{\partial E}{\partial y}\frac{\partial H}{\partial y} + \frac{D_H}{H_\infty}\left(\frac{\partial H}{\partial y}\right)^2\right]$$

$$- \Lambda_1\frac{\partial H}{\partial x} - \Lambda_2\frac{\partial \Lambda_1}{\partial y} + \frac{v\lambda_2}{c_p\gamma}\left(\Lambda_1\frac{\partial \Lambda_1}{\partial y}\frac{\partial^2 \Lambda_1}{\partial x\partial y} + \frac{\partial \Lambda_1}{\partial y}\frac{\partial^2 \Lambda_1}{\partial t\partial y} + \Lambda_2\frac{\partial \Lambda_1}{\partial y}\frac{\partial^2 \Lambda_1}{\partial^2 y}\right). \quad (8)$$

The equation (1), (2), (8) and (4) can be transformed into equivalent partial differential equations using the technique of the similarity solutions. Following variables η, ξ are introduced

$$\eta = y\sqrt{\frac{\alpha}{\nu\xi}};\ \xi = 1 - e^{-\tau^*};\ \tau^* = at, \quad (9)$$

τ^* : dimensionless time. Taking stream function as $\psi = x\sqrt{a\nu\xi}f(\eta, \xi)$ and

$$\theta(\xi, \eta) = (H, H_\infty)/(H_w - H_\infty),\ \phi(\xi, \eta) = (E - E_\infty)/(E_w - E_\infty), \quad (10)$$

where $f(\xi, \eta)$ is the dimensionless stream function. Variable thermal conductivity is considered as $k = k_a(1 + \alpha\theta(\xi, \eta))$ with thermal conductivity parameter given by $\alpha = (k - k_a)/k_a$ [37]. The velocity components are related to the stream function as $\Lambda_1 = \frac{\partial \psi}{\partial y};\ \Lambda_2 = -\frac{\partial \psi}{\partial x}$.

Making use of above defined transformations, equations (1), (2), (8) and (4) looks like

$$\left[\frac{1+\beta}{\gamma} - \frac{\beta}{\xi\gamma}\right]\frac{\partial^3 f}{\partial \eta^3} + \frac{\beta}{\gamma}\left[\left\{\left(\frac{\partial^2 f}{\partial \eta^2}\right)^2 + \frac{\partial^4 f}{\partial \eta^4}\right\} + (1-\xi)\frac{\partial^4 f}{\partial \xi\partial \eta^3} + \frac{\eta}{2}\left(1 - \frac{1}{\xi}\right)\frac{\partial^4 f}{\partial \eta^4}\right]$$

$$+ \xi\left(f\frac{\partial^2 f}{\partial \eta^2} - \left(\frac{\partial f}{\partial \eta}\right)^2\right) + (1-\xi)\left(\frac{\eta}{2}\frac{\partial^2 f}{\partial \eta^2} - \xi\frac{\partial^2 f}{\partial \xi\partial \eta}\right) - M\frac{\partial f}{\partial \eta} = 0, \quad (11)$$

$$\frac{1}{\Pr}\left[\left\{(1 + \alpha\theta) + \frac{4}{3R_D}((1 + \delta\theta)^3)\right\}\frac{\partial^2 \theta}{\partial \eta^2} + \left\{\alpha + \frac{4}{R_D}\delta(1 + \delta\theta)^2)\right\}\left(\frac{\partial \theta}{\partial \eta}\right)^2\right] + \xi f\frac{\partial \theta}{\partial \eta}$$

$$+\frac{\eta}{2}(1-\xi)\frac{\partial\theta}{\partial\eta}-\xi(1-\xi)\frac{\partial\theta}{\partial\xi}+N_b\frac{\partial\phi}{\partial\eta}\frac{\partial\theta}{\partial\eta}+N_t\left(\frac{\partial\theta}{\partial\eta}\right)^2+\frac{Ec}{\gamma\xi^2}[(\xi+\beta)\xi-\beta]\left(\frac{\partial^2 f}{\partial\eta^2}\right)^2$$

$$+\frac{\beta Ec}{\gamma}\left[\left(\frac{\partial f}{\partial\eta}\left(\frac{\partial^2 f}{\partial\eta^2}\right)^2-f\frac{\partial^2 f}{\partial\eta^2}\frac{\partial^3 f}{\partial\eta^3}\right)+(1-\xi)\left(\frac{\partial^2 f}{\partial\eta^2}\frac{\partial^3 f}{\partial\xi\partial\eta^2}-\frac{\eta}{2\xi}\frac{\partial^2 f}{\partial\eta^2}\frac{\partial^3 f}{\partial\eta^3}\right)\right]=0, \quad (12)$$

$$\frac{\partial^2\phi}{\partial\eta^2}+Le\xi\frac{\partial\phi}{\partial\eta}+\frac{N_t}{N_b}\frac{\partial^2\theta}{\partial\eta^2}-Le(1-\xi)\left(\frac{\eta}{2}\frac{\partial\phi}{\partial\eta}-\xi\frac{\partial\phi}{\partial\xi}\right)-\Pr LeRc\phi=0, \quad (13)$$

and restyled boundary conditions are

$$\frac{\partial f}{\partial\eta}(\xi,0)=1,\ f(\xi,0)=\theta(\xi,0)=0,\theta(\xi,0)=1,\ \phi(\xi,0)=1,$$

$$\frac{\partial f}{\partial\eta}(\xi,\infty)\to 0,\ \theta(\xi,\infty)\to 0,\ \phi(\xi,\infty)=0, \quad (14)$$

$$M=\frac{\sigma B^2}{a\rho},\ \Pr=\frac{\upsilon}{\alpha},\ \beta=a\lambda_2,\ \delta=(\theta_w-1),$$

where,

$$\left.\begin{aligned} &M=\frac{\sigma B^2}{a\rho},\ \Pr=\frac{\nu}{\alpha},\ \beta=a\lambda_2,\ \delta=(\theta_w-1),\\ &N_b=\frac{\tau_p D_B(E_w-E_\infty)}{\nu},\ N_t=\frac{\tau_p D_H(H_w-H_\infty)}{\nu H_\infty}\,Ec=\frac{\Lambda_{1x}^2}{c_p(H_w-H_\infty)},\\ &Le=\frac{\nu}{D_B},\ \alpha=\frac{k}{\rho cf},\ Rc=\frac{k_c x}{\Lambda_{1_w}(x)},\ R_D=\frac{k^* a}{4\sigma^* H_\infty^3} \end{aligned}\right\}$$

where, M, Pr, N_b, N_t, Ec, Le, R_D and Rc are parameters/numbers of, respectively, magnetic, Prandtl, Brownian motion, thermophoresis, Eckert, Lewis, Radiation and chemical reaction.

Skin friction Cf_x, Nusselt number Nu_x and Sherwood number Sh_x, are expressed as:

$$Cf_x\,\mathrm{Re}_x^{\frac{1}{2}}\,\xi^{\frac{1}{2}}=\frac{1}{\gamma}\left[(1+\beta)\frac{\partial^2 f}{\partial\eta^2}\beta(1-\xi)\left(\frac{\partial^3 f}{\partial\xi\partial\eta^2}-\frac{1}{2\xi}\frac{\partial^2}{\partial\eta^2}\right)\right]_{\eta=0},$$

$$Nu_x \, \mathrm{Re}_x^{-\frac{1}{2}} \, \xi^{-\frac{1}{2}} = -\left(1 + \frac{4}{3Rd}\,\theta_w^3\right)\frac{\partial \theta}{\partial \eta}|_{\eta=0},$$

$$Sh_x \, \mathrm{Re}_x^{-\frac{1}{2}} \, \xi^{-\frac{1}{2}} = \frac{\partial \phi}{\partial \eta}|_{\eta=0} \, .$$

$\mathrm{Re}_x \, \frac{\Lambda_w(x)x}{\nu}$ is Reynolds number.

3. Numerical Algorithm

In this section, we discuss application of proposed bivariate simple iteration method (BSIM) on nonlinear system of partial differential equations (11)-(13) and its corresponding boundary conditions (14). The BSIM involves the implementation of relaxation on nonlinear system of equations. This is done by assuming all linear functions to be unknown functions while defining nonlinear functions as both known (from a previously defined initial solution that satisfies the boundary conditions) and unknown. To apply this on nonlinear system, the function with highest derivative is made unknown while the other function(s) is (are) assumed to be known. We however note that this rule applies only to the functions that define the specific equation being solved. For example, the term $\phi' \theta'$ in equation (12) appears. We apply rules of the BSIM by assuming ϕ' to be a known function and θ' to be unknown function. This is done because equation (12) represents the energy equation and is defined in terms of θ and its derivatives. Following the same analogy given, we obtain

$$[a_1] f_{r+1}^{iv} + (a_2) f_{r+1}''' + [a_3] f_{r+1}'' + [a_4] f_{r+1}' = (-(1-\xi))\frac{\partial f_{r+1}'''}{\partial \xi} + (\xi^2(1-\xi))\frac{\partial f_{r+1}'}{\partial \xi}, \quad (15)$$

$$[b_1]\theta_{r+1}'' + [b_2]\theta_{r+1}' = \xi^3(1-\xi)\frac{\partial \theta_{r+1}}{\partial \xi} + b_3, \quad (16)$$

$$\phi_{r+1}'' + [c_1]\phi_{r+1}' - \mathrm{Pr}\, LeRc\phi_{r+1} = -Le\xi(1-\xi)\frac{\partial \phi_{r+1}}{\partial \xi} + c_2, \quad (17)$$

where coefficient functions in $(\cdots)$ and $[\cdots]$ denote scalar and vector

functions, respectively and

$$a_1 = \frac{\beta}{\gamma}\left(\xi f_r + \frac{\eta}{2}(\xi - 1)\right),\ a_2 = \frac{1}{\gamma}((1+\beta)\xi - \beta),$$

$$a_3 = \frac{\xi\beta}{\gamma} f_r'' + \xi(1-\xi)\frac{\eta}{2} + \xi^2 f_r,\ a_4 = -\xi^2 f_r - \xi M,$$

$$b_1 = \frac{\xi^2}{\Pr}\left((1+\alpha\theta_r) + \frac{4}{3R_D}\left((1+\delta\theta_r)^3\right)\right),$$

$$b_2 = \frac{\xi^2}{\Pr}\left(\alpha + \frac{4}{3R_D}\delta\left((1+\delta\theta_r)^2\right)\right)\theta_r' + \xi^3 f_{r+1} + \frac{\xi^2\eta}{2}(1-\xi) + \xi^2 N_{b\phi' r} + \xi^2 N_t \theta_r',$$

$$b_3 = -\frac{Ec}{\gamma}((\xi+\beta)\xi - \beta) f_{r+1}''^2 -$$

$$\frac{\xi^2\beta Ec}{\gamma}((f_{r+1}' f_{r+1}''^2 - f_{r+1} f_{r+1}'' f_{r+1}''') + (1-\xi) f_{r+1}'' \frac{\partial f_{r+1}''}{\partial\xi} - \frac{(1-\xi)\eta}{2\xi} f_{r+1}'' f_{r+1}'''),$$

$$c_1 = Le\xi f_{r+1} - Le(1-\xi)\frac{\eta}{2},\ c_2 = -\frac{N_t}{N_b}\theta_{r+1}''.$$

The system (15)-(17) represents a decoupled system of linear partial differential equations which can be solved using various methods. The BSIM however, involves the use of Chebyshev spectral collocation method to solve the system. Details of Chebyshev spectral collocation method can be obtained in following literature Tang [38], Trefethen [39] and Canuto et al. [40]. Solving the system (15)-(17) that is defined on the physical domains $\eta \in [0, \infty)$ and $\xi \in [0, \infty)$ require transformation to finite domains $x \in [-1, 1]$ and $t \in [-1, 1]$. We approximate the solutions to $f(x, t)$, $\theta(x, t)$ and $\phi(x, t)$ using the Lagrange interpolating polynomials

$$f(x, t) \approx \sum_{i=0}^{M_x}\sum_{j=0}^{M_t} f(x_i, t_j) L_i(x) L_j(t), \tag{18}$$

$$\theta(x, t) \approx \sum_{i=0}^{M_x}\sum_{j=0}^{M_t} \theta(x_i, t_j) L_i(x) L_j(t), \tag{19}$$

$$\phi(x, t) \approx \sum_{i=0}^{M_x} \sum_{j=0}^{M_t} \phi(x_i, t_j) L_i(x) L_j(t), \tag{20}$$

where L_i and L_j are called Lagrange cardinal functions that are defined as

$$L_i(x) = \prod_{i=0,\ i \neq k}^{M_x} \frac{x - x_k}{x_i - x_k},$$

$$L_j(t) = \prod_{j=0,\ j \neq k}^{M_t} \frac{t - t_k}{t_i - t_k},$$

where

$$L_i(x_k) = \delta_{ik} = \begin{cases} 0 \text{ if } i \neq k \\ \\ 1 \text{ if } i \neq k \end{cases},$$

$$L_j(t_k) = \delta_{jk} = \begin{cases} 0 \text{ if } j \neq k \\ \\ 1 \text{ if } j \neq k \end{cases}, \tag{21}$$

We take Gauss-Chebyshev-Lobatto points as grid-points x_i and t_j due to their ease in converting continuous time and special derivatives into discrete derivatives. The points are given as

$$x_i = \cos \frac{\pi i}{M_x},\ i = 0, 1, \cdots, M_x,$$

$$t_j = \cos \frac{\pi j}{M_t},\ i = 0, 1, \cdots, M_t \tag{22}$$

Differentiation matrices (denoted by D in space and d in time) are used to collocate in form

$$\frac{\partial f^{(p)}}{\partial x^{(p)}} \Big|_{x_i, t_j} = D^{(p)} F_i, \frac{\partial f}{\partial t} \Big|_{x_i, t_j} = \sum_{j=0}^{M_t} d_{ij} F_j,$$

$$\frac{\partial^{(p)}\theta}{\partial x^{(p)}}\Big|_{x_i,\,t_j} = D^{(p)}\Theta_i, \frac{\partial\theta}{\partial t}\Big|_{x_i,\,t_j} = \sum_{j=0}^{M_t} d_{ij}\Theta_j,$$

$$\frac{\partial^{(p)}\phi}{\partial x^{(p)}}\Big|_{x_i,\,t_j} = D^{(p)}\Phi_i, \frac{\partial\phi}{\partial t}\Big|_{x_i,\,t_j} = \sum_{j=0}^{M_t} d_{ij}Ph_{ij}, \tag{23}$$

where F, Θ and Φ are vectors of the form

$$F = [f(x_0, t_j), f(x_1, t_j), \cdots, f(x_{N_x}, t_j)]^T,$$

$$\Theta = [\theta(x_0, t_j), \theta(x_1, t_j), \cdots, \theta(x_{N_x}, t_j)]^T,$$

$$\Phi = [\phi(x_0, t_j), \phi(x_1, t_j), \cdots, \phi(x_{N_x}, t_j)]^T. \tag{24}$$

Applying the representations given by (23) on the decoupled linear system (15)-(17), we obtain

$$[[a_{1,i}]D^4 + (a_2)D^3 + [a_{3,i}]D^2]F_{r+1,i} + (1-\xi)\sum_{j=0}^{M_{t-1}} d_{ij}D^3F_{r+1,i} \tag{25}$$

$$-(\xi^2(1-\xi))\sum_{j=0}^{M_{t-1}} d_{ij}DF_{r+1,i} = R_{1,i},$$

$$[[b_{1,i}]D^2 + [b_{2,i}]D]\Theta_{r+1,i} - (\xi^3(1-\xi))\sum_{j=0}^{M_{t-1}} d_{ij}I\,\Theta_{r+1,i}R_{2,i}, \tag{26}$$

$$[D^2[c_{1,i}]D - (\mathrm{Pr}\,LeR_c)\Phi_{r+1,i} - (Le\xi(1-\xi))\sum_{j=0}^{M_{t-1}} d_{ij}I\Phi_{r+1,i}R_{3,i}, \tag{27}$$

where I is an identity matrix and

$$R_{1,i}(1-\xi)d_{i,M_t}(D^3F_{M_t}) + (\xi^2(1-\xi))d_{i,M_t}(DF_{M_t}),$$

$$R_{2,i} = (\xi^3(1-\xi))d_{i,M_t}\Theta_{M_t} + b_3,$$

$$R_{3,i} = (Le\xi(1-\xi))d_{i,M_t}\Phi_{M_t} + c_2.$$

3.1. Convergence

We test the convergence of the BSIM by calculating the error between solutions of successive iterations. When the error between the solutions reaches a point where further increase in iterations has no significant effect, we say our method converges. We took 10 grid-points in η and ξ directions, respectively. Grid independent test revealed that these are adequate in generating accurate solution. For this the value of parameters is considered as $\beta = 0.1, \gamma = 0.2, M = 0.2, \Pr = 5, \alpha = 0.5, Rd = 10, \delta = 0.5, N_b = 0.2, N_t = 0.05,$ $Ec = 0.2$, $Le = 10$ and $R_c = 0.1$. These values are also used to sketch the graphs. The solution error norms are computed as;

$$\| F \|_\infty = \max_{0 \le i \le M_t} \| F_{r+1,i} - F_{r,i} \|_\infty,$$

$$\| \Theta \|_\infty = \max_{0 \le i \le M_t} \| \Theta_{r+1,i} - \Theta_{r,i} \|_\infty,$$

$$\| \Phi \|_\infty = \max_{0 \le i \le M_t} \| \Phi_{r+1,i} - \Phi_{r,i} \|_\infty. \tag{28}$$

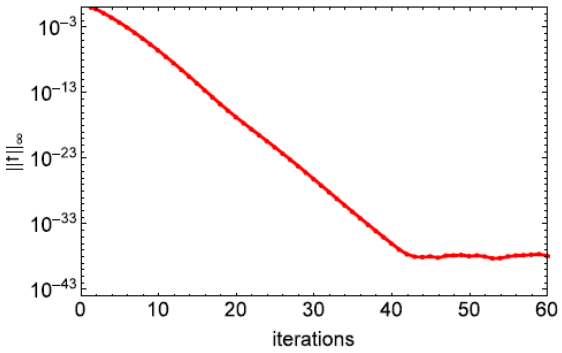

Figure 1. Solution error of f at $\xi = 0.4$.

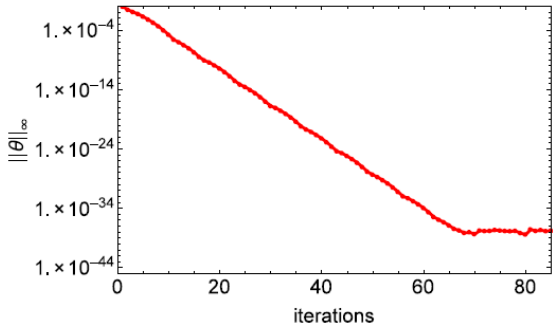

Figure 2. Solution error θ at $\xi = 0.4$.

Figures 1 to 3 display the convergence of the BSIM. We observe that the error reduces to as little as 10^{-40} as iterations increase in all three figures until a certain point where the error seems to stabilize. In Figure 1, we observe that convergence occurs after 40 iterations while it takes about 65 iterations to converge in both figures 2 and 3. This suffices the convergence of proposed method.

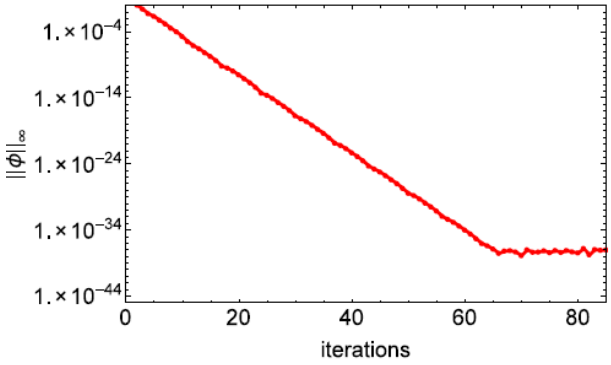

Figure 3. Solution error norm of ϕ at $\xi = 0.4$.

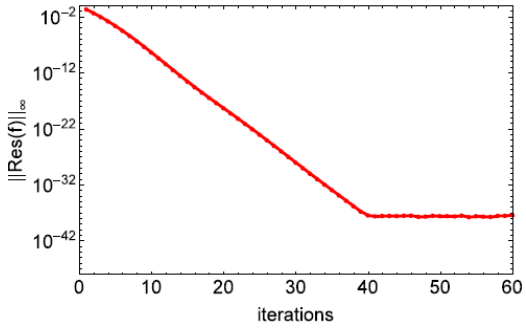

Figure 4. Residual of f at $\xi = 0.4$.

3.2. Accuracy

In verifying the accuracy of BSIM, we calculate the residual error norms by substituting the obtained approximate solutions in original system of differential equations. Residual error norms are a measure which signifies the closeness of approximate solutions to analytical solutions of considered system of differential equations. We define the residual error norms as

$$\mathrm{Res}(F) = \max_{0\le i\le M_t} \| \left[\frac{1+\beta}{\gamma} - \frac{\beta}{\xi\gamma}\right] f_r''' + \frac{\beta}{\gamma}\left[\{(f_r''')^2 + f_i f_i^{iv}\} + (1-\xi)\frac{\partial f_i'''}{\partial \xi} + \frac{\eta}{2}\left(1-\frac{1}{\xi}\right) f_i^{iv}\right]$$

$$+ (1-\xi)\left(\frac{\eta}{2} f_i'' - \xi\frac{\partial f_i'}{\partial \xi}\right) - \xi(f_i f_i'' - (f_i')^2) - M f_i' \|_\infty, \tag{29}$$

$$\mathrm{Res}(\Theta) = \max_{0\le i\le M_t} \| \frac{1}{\mathrm{Pr}}\left[\left\{(1+\alpha\theta_i) + \frac{4}{3R_D}((1+\delta\theta_i)^3)\right\}\theta_i'' + \left\{\alpha + \frac{4}{R_D}\delta((1+\delta\theta_i)^2)\right\}(\theta_i')^2\right]$$

$$+ \xi f_i\theta_i' + \frac{\eta}{2}(1+\xi)\theta_i' - \xi(1-\xi)\frac{\partial\theta_i}{\partial\xi} + Nb\phi_i'\theta_i' + N_t(\theta_i')^2 + \frac{Ec}{\gamma\xi^2}[(\xi+\beta)\xi - \beta]$$

$$(f''_i) + \frac{\beta Ec}{\gamma}\left[(f_i')(f_i'')^2 - f_i f_i'' f_i''') + (1-\xi)\left(f_i''\frac{\partial f_i''}{\partial\xi} - \frac{\eta}{2\xi} f_i'' f_i'''\right)\right] \|_\infty, \tag{30}$$

$$\mathrm{Res}(G) = \max_{0\le i\le M_t} \| \phi_i'' + Le\xi f_i\phi_i' + \frac{N_t}{N_b}\theta_i'' - Le(1-\xi)\left(\frac{\eta}{2}\phi_i' - \xi\frac{\partial\phi_i}{\partial\xi}\right) - \mathrm{Pr}\, Le R_c\phi_i \|_\infty. \tag{31}$$

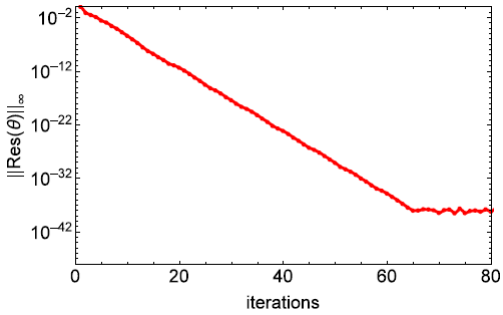

Figure 5. Residual of θ at $\xi = 0.4$.

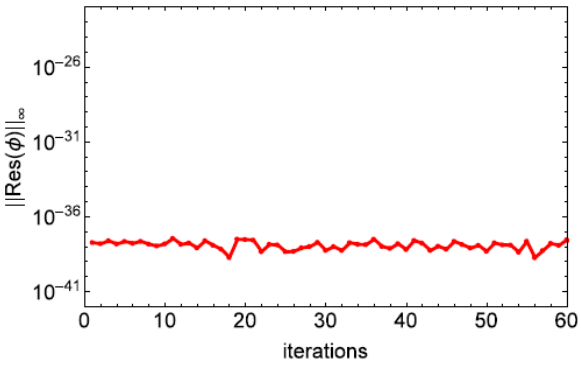

Figure 6. Residual of ϕ at $\xi = 0.4$.

It is observed from figures 4 to 6 that the residual errors of numerical solutions to the equations 11-13 are about 10^{-40} Coupled with the knowledge that few grid points in space and time were used to generate these solutions (10 in each), this suggests that the BSIM is an efficient method capable of giving accurate solutions with errors small enough. We also examine that the residual errors of figures 4 and 5 converge linearly as the number of iterations increase while we note that figure 6 shows consistent residual error from the start. This is because equation (13) is linear in ϕ and its derivatives as the solution for f and θ are known before solving the third equation.

4. Result Analysis

To report the influence of flow parameters on dimensionless velocity

$f'(\eta, \xi)$, temperature $\theta(\eta, \xi)$ and nanoparticle concentration $\phi(\eta, \xi)$ numerical solution of system of governing differential equations, obtained by bivariate simple iteration method BSIM, are replicated in graphs.

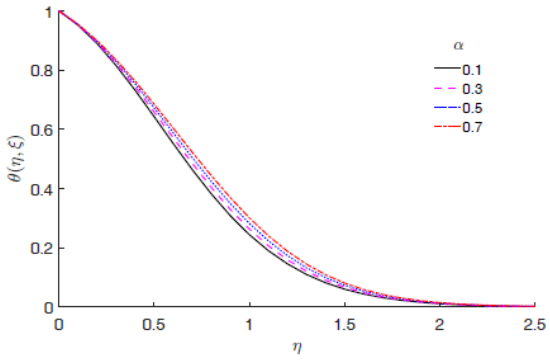

Figure 7. Effect of Thermal Conductivity α on θ.

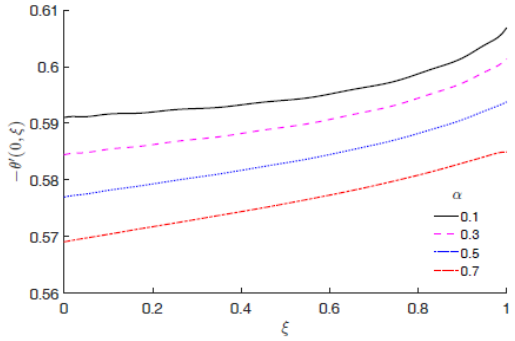

Figure 8. Effect of Thermal Conductivity α on θ'.

Figures 7 and 8 are the graphical representation of numerical results of fluid temperature $\theta(\eta, \xi)$ and local nusselt number $\theta'(0, \xi)$ respectively, with different thermal conductivity parameter. Figure 7 disclose that the effect of thermal conductivity parameter is to enhance the temperature. Consequently a significant reduction in heat transfer at the surface is observed from figure 8. Coolant materials having small thermal conductivity give a faster cooling rate. This result is in agreement with the result reported in Srinivas Reddy et al. [41].

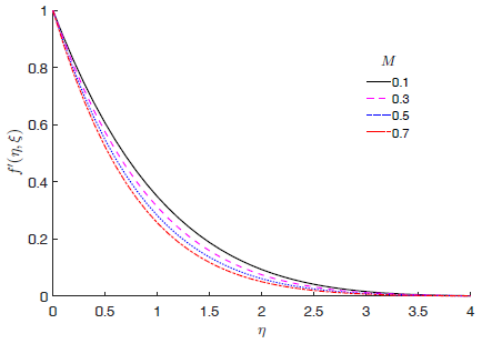

Figure 9. Effect of magnetic parameter M on f'.

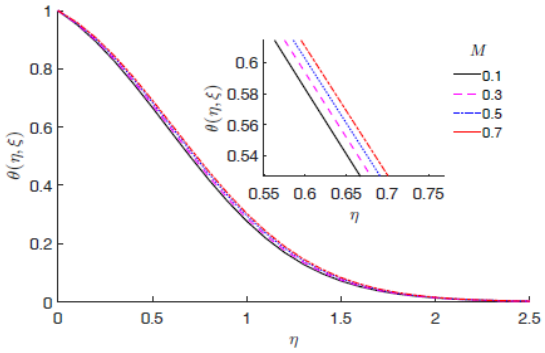

Figure 10. Effect of magnetic parameter M on θ.

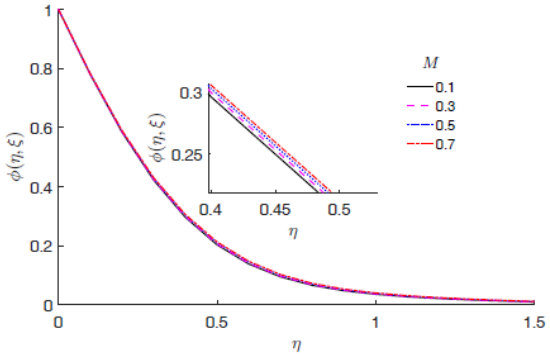

Figure 11. Effect of magnetic parameter M on ϕ'.

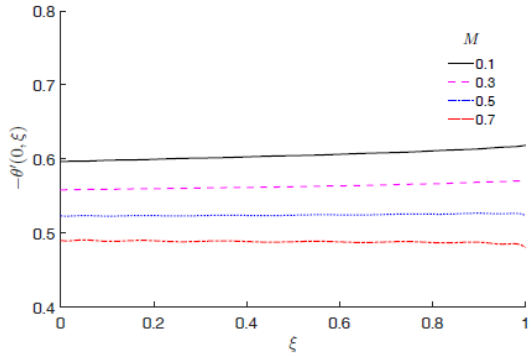

Figure 12. Effect of magnetic parameter M on θ'.

Behaviour of velocity, temperature and concentration profiles for different values of M are shown graphically in Figure 9, 10 and 11, respectively. One can observe that, with increase in the value of M, there is a decrease in velocity profile and an increase in the temperature and concentration profiles. Figure 12 conveys a 8 decrease in rate of heat transfer with an increase in magnetic parameter, evincing the increase in temperature profile observed in the boundary layer. The presence of magnetic field across the flow field creates a barrier, termed as Lorentz force, which opposes the flow fields and in turn reduces the velocity of the fluid proliferating nanoparticle concentration in boundary layer region, decreasing the rate of heat flow and increasing the temperature near the boundary layer. Figures 13, 14 and 15 constitutes the profiles of velocity, temperature and concentration, respectively, for different values of relaxation to retardation time λ_1. The velocity profile appears to reduce with an increase in λ_1 whereas, an increase in temperature and concentration is obtained.

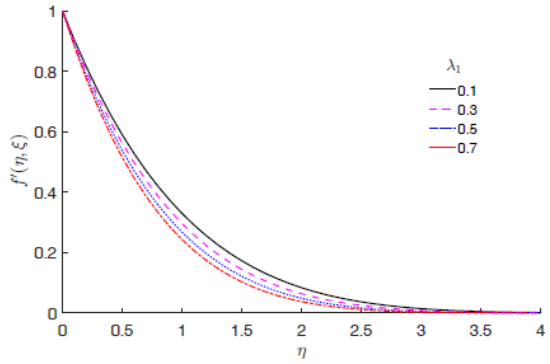

Figure 13. Effect of relaxation to retardation time parameter λ_1 on f'.

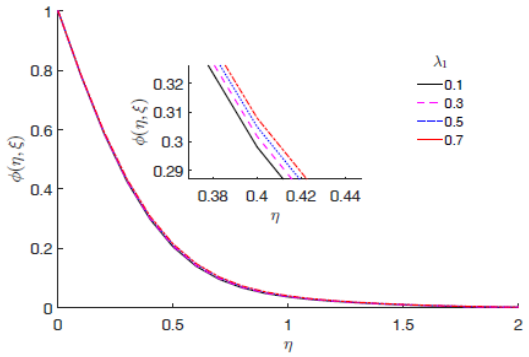

Figure 14. Effect of relaxation to retardation time parameter λ_1 on ϕ.

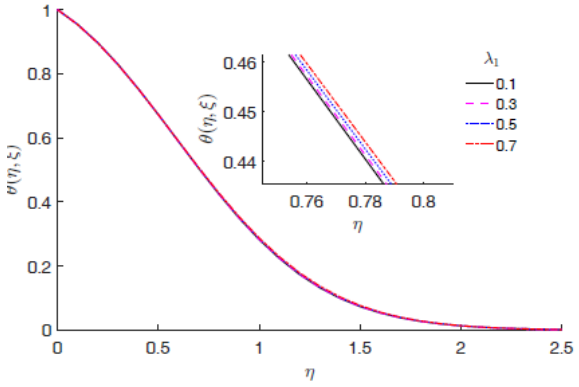

Figure 15. Effect of relaxation to retardation time parameter λ_1 on θ.

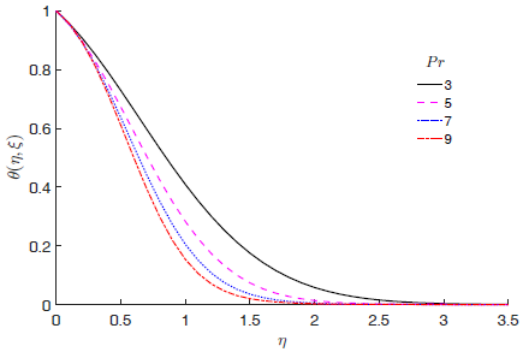

Figure 16. Effect of Prandtl Number *Pr* on θ.

Figure 16 represents the consequence due to change in Prandtl number on Temperature. The plot shows that with increase in Prandtl number the temperature decreases, it concede from the definition of Prandtl number, as an increase in Prandtl number reduces the thermal conductivity. From Figure 17 and 18, it is clear that, with increase in Prandtl number the nanoparticle concentration increases and rate of change in nanoparticle concentration flux at surface increases with Prandtl number and time. Figure 19 is drawn to illustrate the effects of Eckert number *Ec* on temperature distribution. A gradual upsurge in Eckert number results in an increase in the temperature profile. The ratio of advective mass transport over heat dissipation is termed as, Eckert number. Thus, an increase in Eckert number should result in decreased heat dissipation coercing a rise in boundary layer temperature. Figure 20 and 21 depict the swing of boundary layer temperature and concentration for distinct values of Lewis number, Le. It can be observed from the plots that, with increase in Lewis number both, temperature and nanopartical concentration decreases.

Figure 22 and 23 portrait the trends of θ and ϕ profiles, respectively, for various values of thermophoretic parameter, N_t. With increase in thermophoretic parameter, an increase in temperature and concentration near boundary layer is obtained. Figure 24 and 25, reveal the behaviour of θ and ϕ profiles, respectively, for different values of N_b. From Figure 24, it is tangible that an increase in N_b, escalate mutual collision of nanoparticles and hence fosters the temperature profile. Moreover, Figure 25, infers that

with increase in Brownian motion parameter, there is a depletion of nanoparticle concentration boundary layer thickness.

From Figure 26, it is clear that temperature profile is a decreasing function of conduction R_D. As a matter of fact, a proliferation in thermal conduction radiation parameter decreases the mean absorption coefficient, which enhances the divergence of radiative heat flux. Thus, an increase in radiation parameter and a decrease in thermal absorption, culminates to an overall decrease in the thermal profile and its allied boundary layer thickness. Heat transfer decreases at the sheet drastically for small values of conduction radiation parameter R_D (see figure 27). $R_D \to \infty$ implies no radiation effect. Figure 28, shows the influence of parameter Rc, on ϕ profile. It is found that, an increase in value of Rc, yields a decrease in nanoparticle concentration. Larger values of Rc results in less diffusion, i.e. less chemical molecular diffusivity. Therefore, the distribution of concentration profile decreases with an increase in reaction parameter.

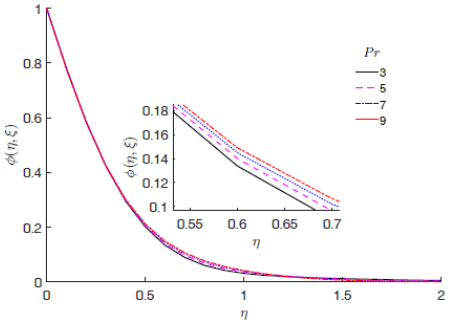

Figure 17. Effect of Prandtl Number Pr on ϕ.

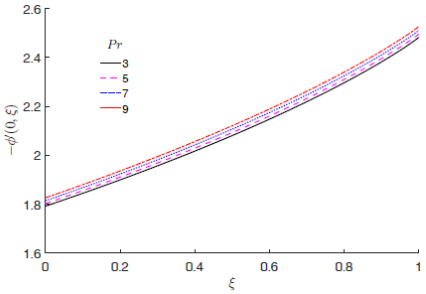

Figure 18. Effect of Prandtl Number Pr on $\phi'(0, \xi)$.

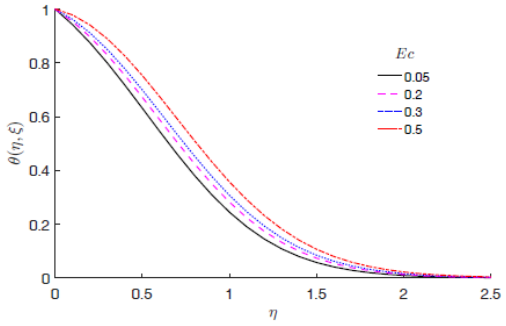

Figure 19. θ profiles with Ec.

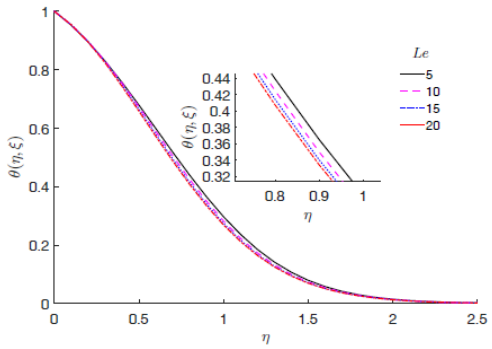

Figure 20. Variation of θ profiles with *Le*.

Figures 29 and 30 depict the alteration of θ and ϕ within boundary layer for various values of dimensionless time $\xi\xi = 0$ and $\xi = 1$) correspond, respectively, initial unsteady and final steady state. It is make out that θ and ϕ profiles decrease in the boundary region with the increase of distance from the stretching surface.

We notice from figures 29 and 30 that the temperature and concentration boundary layer thickness decrease as time progresses until the steady state is reached.

5. Conclusions

The applicability of bivariate simple iteration method BSIM is studied on unsteady boundary layer flow of incompressible Jeffrey nanofluid over an impulsively stretching plate combining the effects of variable thermal conductivity, nonlinear radiation and chemical reaction. Jeffrey fluid takes

into account the impact of the ratio of stress relaxation to retardation times and retardation time. The proposed method is shown to be convergent and efficient in giving accurate solutions even in few number of grid points. Some of the notable findings in present study are listed as

i. Thermal boundary layer thickness decreases with the increase of ratio of relaxation to retardation times. This decrease in the temperature of fluid is due to presence of viscous dissipation.

ii. Fluid temperature and nanoparticle concentration in boundary layer region decrease with time.

iii. Heat transfer decreases with an increase in thermal conductivity parameter.

iv. Strength of chemical reaction modifies the diffusion rate, hence a decrease in nanoparticle concentration occurs with chemical reaction parameter.

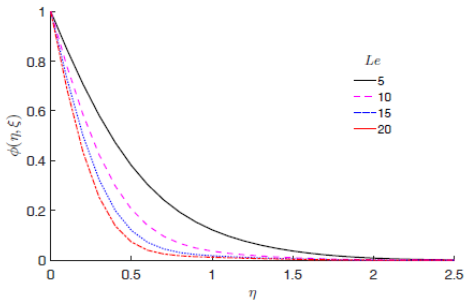

Fgure 21. Impact of Le on ϕ.

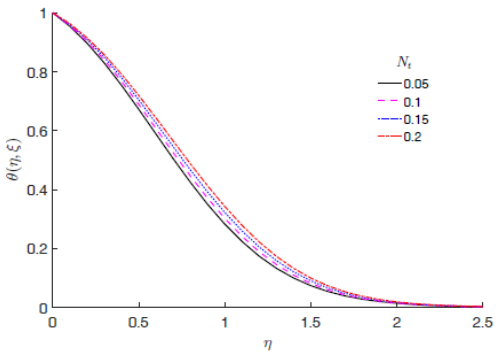

Figure 22. θ profiles with N_t.

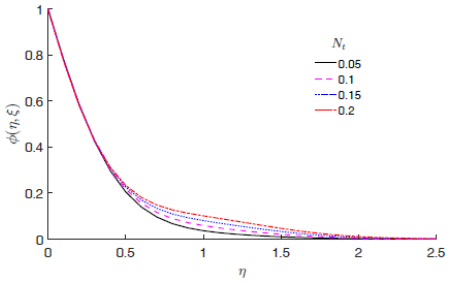

Figure 23. Effect of N_t on ϕ.

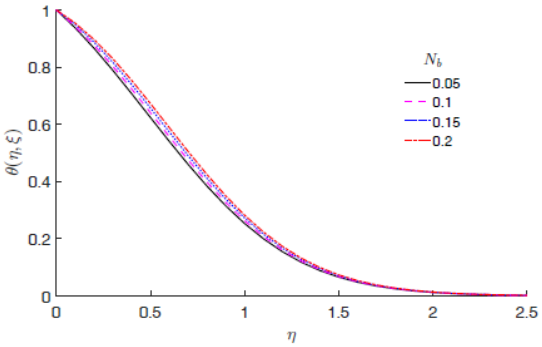

Figure 24. Effect of N_b on θ.

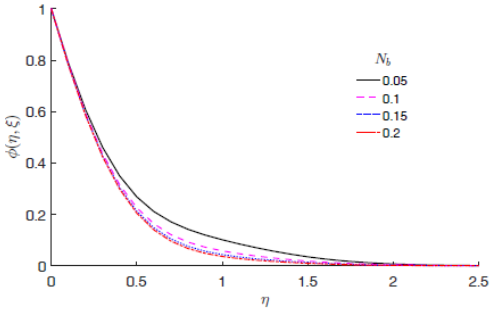

Figure 25. Effect of N_b on ϕ.

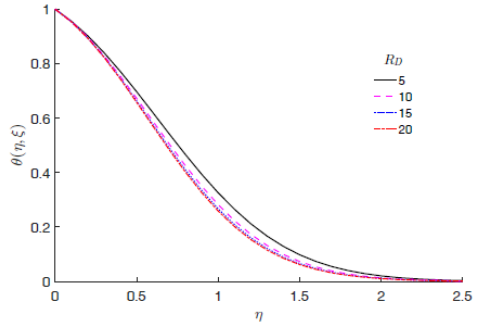

Figure 26. Effect of R_D on θ.

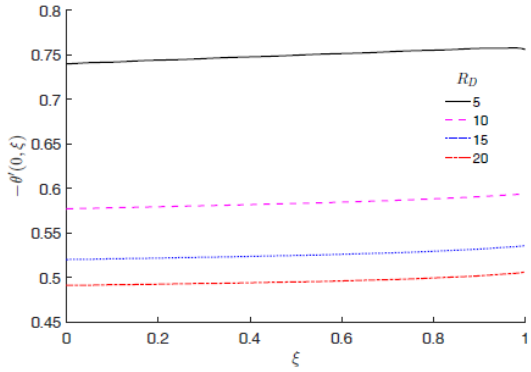

Figure 27. Impact of R_D on θ' (0, ξ).

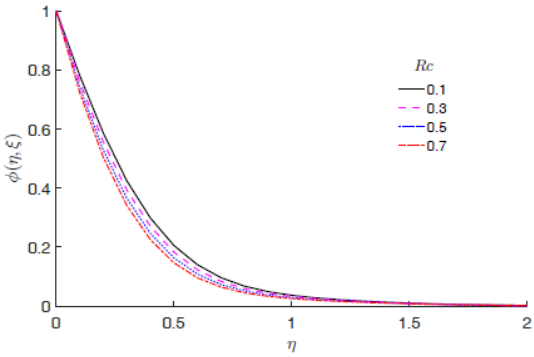

Figure 28. Effect of Rc on ϕ.

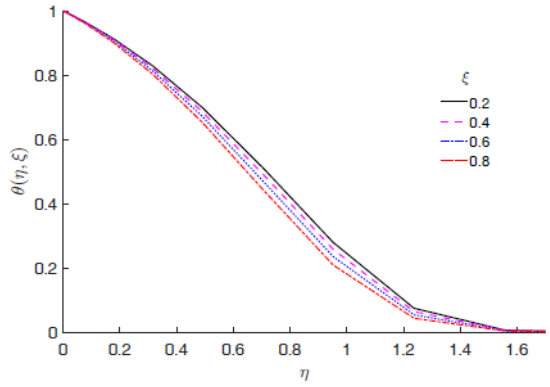

Figure 29. Impact of ξ on θ.

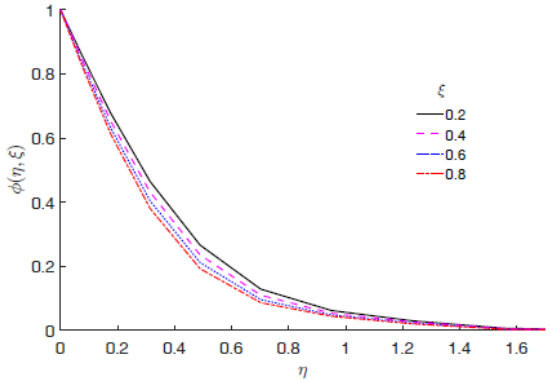

Figure 30. Effect of ξ on ϕ.

References

[1] T. Hayat and M. Mustafa, Influence of Thermal Radiation on the Unsteady Mixed Convection Flow of a Jeffrey Fluid over a Stretching Sheet, Zeitschrift fur Naturforsch. A, 65(8-9) (2010), 711-719.

[2] S. Nadeem, S. Zaheer and T. Fang, Effects of thermal radiation on the boundary layer ow of a Jeffrey uid over an exponentially stretching surface, Numer. Algorithms 57(2) (2011), 187-205.

[3] M. A. A. Hamad, S. M. AbdEl-Gaied and W. A. Khan, Thermal Jump Effects on Boundary Layer Flow of a Jeffrey Fluid Near the Stagnation Point on a Stretching/Shrinking Sheet with Variable Thermal Conductivity, J. Fluids, vol. 2013, Article id 749271, 8 pages, 2013.

[4] R. U. Haq, S. Nadeem, Z. H. Khan and T. G. Okedayo, Convective heat transfer and MHD effects on Casson nanofluid flow over a shrinking sheet, Cent. Eur. J. Phys. 12(12) (2014), 862-871.

[5] F. M. Abbasi, S. A. Shehzad, T. Hayat, A. Alsaedi and M. A. Obid, Influence of heat and mass flux conditions in hydromagnetic flow of Jeffrey nanofluid, AIP Adv., vol. 5(3), article id 037111,12 pages, 2015.

[6] T. Hayat, M. Waqas, S. A. Shehzad and A. Alsaedi, MHD stagnation point flow of Jeffrey fluid by a radially stretching surface with viscous dissipation and Joule heating, J. Hydrol. Hydromechanics 63(4) (2015), 311-317.

[7] K. G. Kumar, N. G. Rudraswamy, B. J. Gireesha and M. R. Krishnamurthy, Influence of nonlinear thermal radiation and viscous dissipation on three-dimensional flow of Jeffrey nano fluid over a stretching sheet in the presence of Joule heating, Nonlinear Eng. 6(3) (2017), 207-219.

[8] T. Hayat, T. Muhammad, S. A. Shehzad and A. Alsaedi, Three-Dimensional Flow of Jeffrey Nanofluid with a New Mass Flux Condition, J. Aerosp. Eng., vol. 29(2), article id 04015054, 8 pages, 2016.

[9] T. Abbas, M. M. Bhatti and M. Ayub, Aiding and opposing of mixed convection Casson nanofluid flow with chemical reactions through a porous Riga plate, Proc. Inst. Mech. Eng. Part E J. Process Mech. Eng. 232(5) (2018), 519-527.

[10] M. I. Anwar, N. Tanveer, M. Z. Salleh and S. Shafie, Diffusive effects on hydrodynamic Casson nanofluid boundary layer flow over a stretching surface, J. Phys. Conf. Ser., vol 890, article id 012047, 8 pages, 2017.

[11] M. M. Rashidi, N. Vishnu Ganesh, A. K. Abdul Hakeem and B. Ganga, Buoyancy effect on MHD flow of nanofluid over a stretching sheet in the presence of thermal radiation, J. Mol. Liq. 198 (2014), 234-238.

[12] G. S. Seth, G. K. Mahato and J. K. Singh, Effects of Hall Current and Rotation on MHD Couette Flow of Class-II, J. Int. Acad. Phys. Sci. 15(1) (2011), 213-230.

[13] H. Masuda, A Ebata, K. Teramae and N. Hishinuma, Alteration of thermal conductivity and viscosity of liquid by dispersing ultra-fine particles, Netsu Bussei 7(4) (1993), 227-233.

[14] S. U. S. Choi and J. A. Eastman, Enhancing thermal conductivity of fluids with nanoparticles, Proc. ASME Int. Mech. Eng. Congr. Expo. 66 (1995), 99-105.

[15] F. Shahzad, M. Sagheer and S. Hussain, Numerical simulation of magneto hydrodynamic Jeffrey nanofluid flow and heat transfer over a stretching sheet considering Joule heating and viscous dissipation, AIP Advances, vol 8, article id 065316, 16 pages, 2018.

[16] F. M. Abbasi, S. A. Shehzad, T. Hayat and M. S. Alhuthali, Mixed convection flow of Jeffrey nanofluid with thermal radiation and double stratification, J. Hydrodynamics Ser. B 28(5) (2016), 840-849.

[17] T. Hayat, A. Aziz, T. Muhammad and A. Alsaedi, A revised model for Jeffrey nanofluid subject to convective condition and heat generation/absorption, PLoS One, vol 12(2), article id e0172518,22 pages, 2017.

[18] T. Hayat, A. Aziz, T. Muhammad and A. Alsaedi, Active and passive controls of Jeffrey nanofluid flow over a nonlinear stretching surface, Results Phys. 7 (2017), 4071-4078.

[19] S. A. Shehzad, Z. Abdullah, A. Alsaedi, F. M. Abbasi and T. Hayat, Thermally radiative three dimensional flow of Jeffrey nanofluid with internal heat generation and magnetic field, J. Magn. Magn. Mater. 397 (2016), 108-114.

[20] T. Hussain, S. A. Shehzad, T. Hayat, A. Alsaedi, F. Al-Solamy and M. Ramzan, Radiative hydromagnetic flow of Jeffrey nanofluid by an exponentially stretching sheet, PLoS One, vol 9(8), article id e103719, 9 pages, 2014.

[21] M. M. Bhatti, A. Zeeshan and R. Ellahi, Simultaneous effects of coagulation and variable magnetic field on peristaltically induced motion of Jeffrey nanofluid containing gyrotactic microorganism, Microvasc. Res. 110 (2017), 32-42.

[22] A. Gul, I. Khan and S. S. Makhanov, Entropy generation in a mixed convection Poiseulle flow of molybdenum disulphide Jeffrey nanofluid, Results Phys. 9 (2018), 947-954.

[23] W. M. Hasona, A. A. El-Shekhipy and M. G. Ibrahim, Combined effects of magneto hydrodynamic and temperature dependent viscosity on peristaltic flow of Jeffrey nanofluid through a porous medium: Applications to oil refinement, Int. J. Heat Mass Transf. 126 (2018), 700-714.

[24] M. Khan, A. Shahid, M. Y. Malik, T. Salahuddin, Thermal and concentration diffusion in Jeffery nanofluid flow over an inclined stretching sheet: A generalized Fourier's and Fick's perspective, J. Molecular Liquids, vol 251, pp 7 - 14, 2018, doi:10.1016/j.molliq.2017.12.001

[25] S. Saleem, Hunza Rafiq, A. Al-Qahtani, Mohamed Abd El-Aziz, M. Y. Malik and I. L. Animasaun, Magneto Jeffrey Nanofluid Bioconvection over a Rotating Vertical Cone due to Gyrotactic Microorganism, Mathematical Problems in Engineering, vol. 2019, Article ID 3478037, 11 pages, 2019.

[26] D. Pal, S. Mondal and H. Mondal, Entropy generation on MHD Jeffrey nanofluid over a stretching sheet with nonlinear thermal radiation using spectral quasilinearisation method, Int. J. Ambient Energy, 2019, https://doi.org/10.1080/01430750.2019.1614984

[27] F. Ali, S. Murtaza, I. Khan, N.A. Sheikh and K. S. Nisar, Atangana Baleanu fractional model for the flow of Jeffrey nanofluid with diffusion-thermo effects: applications in engine oil. Adv Differ Equations, 2019, article number-346, 21 pages, 2019.

[28] M. S. Ansari, V. M. Magagula and M. Trivedi, Jeffrey nanofluid flow near a Riga plate: spectral quasilinearisation approach, Heat Transfer Asian Research, 2020, DOI: https://doi.org/10.1002/htj.21673.

[29] N. Bachok, A. Ishak and I. Pop, Unsteady boundary-layer flow and heat transfer of a nanofluid over a permeable stretching/shrinking sheet, Int. J. Heat Mass Transfer 55(7-8) (2012), 2102-2109.

[30] M. S. Khan, I. Karim, L. E. Ali and A. Islam, Unsteady MHD free convection boundary layer flow of a nanofluid along a stretching sheet with thermal radiation and viscous dissipation effects, Int. Nano Letters 2, article number-24, 9 pages, 2012.

[31] M. Mustafa, T. Hayat and A. Alsaedi, Unsteady boundary layer flow of nanofluid past an impulsively stretching sheet, J. Mechanics 29 (2013), 423-432.

[32] O. A. Beg, M. S. Khan, I. Karim, M. M. Alam and M. Ferdows, Explicit numerical study of unsteady hydromagnetic mixed convective nanofluid flow from an exponentially stretching sheet in porous media, Appl. Nanosci. 4(8) (2014), 943-957.

[33] S. S. Motsa and M. S. Ansari, Unsteady boundary layer flow and heat transfer of Oldroyd-*B* nanofluid towards a stretching sheet with variable thermal conductivity, Thermal Sci. 19 (2015), 239-248.

[34] M. Madhu, N. Kishan and A. J. Chamkha, Unsteady flow of a Maxwell nanofluid over a stretching surface in the presence of magneto hydrodynamic and thermal radiation effects, Propul. Power Res. 6(1) (2017), 31-40.

[35] M. S. Ansari, S. S. Motsa and M. Trivedi, A New Numerical Approach to MHD Maxwellian Nanofluid Flow Past an Impulsively Stretching Sheet, J. Nanofluids 7(3) (2018), 449-459.

[36] P. Rana, N. Shukla, O. A. Beg, A. Kadir and B. Singh, Unsteady electromagnetic radiative nanofluid stagnation-point flow from a stretching sheet with chemically reactive nanoparticles, Stefan blowing effect and entropy generation, Proc. IMECHE-Part N: J. Nanomaterials, Nanoengineering and Nanosystems 232(2-3) (2018), 69-82.

[37] M. Ramzan, M. Bilal, S. Kanwal and J. D. Chung, Effects of Variable Thermal Conductivity and Non-linear Thermal Radiation Past an Eyring Powell Nanofluid Flow with Chemical Reaction, Communications in Theoretical Physics 67 (2017), 723-731.

[38] J. Shen and T. Tang, Spectral and high-order methods with applications, Science press, Beijing, 2006.

[39] L. N. Trefethen, Spectral Methods in MATLAB, SIAM, vol. 10. 2000.

[40] C. Canuto, M. Y. Hussaini, A. Quarteroni and T. A. Zang, Spectral Method in Fluid Dynamics, Springer, Berlin, Heidelberg, 1988.

[41] C. Srinivas Reddy, K. Naikoti and M. M. Rashidi, MHD flow and heat transfer characteristics of Williamson nanofluid over a stretching sheet with variable thickness and variable thermal conductivity, Transactions of A. Razmadze Mathematical Ins. 171 (2017), 195-211.